The Cold-Core Temperature Structure in a Tropical Easterly Wave

MARY ANN JENKINS

Department of Earth and Atmospheric Science, York University, North York, Ontario, Canada

(Manuscript received 1 June 1993, in final form 16 September 1994)

ABSTRACT

The purpose of this study is to identify what effects are responsible for the observed temperature field, in particular the lower-level cold core, in the trough region of a convectively active tropical easterly wave disturbance. GATE Phase III A/B- and B-scale data were used in the analysis, and the divergence equation, a first-order balance condition proposed by Cho and Jenkins applicable to slowly evolving or near-steady-state large-scale convectively active tropical circulation systems, and the standard nonlinear and linear balance equations were chosen as the framework in which to assimilate the observational data in order to understand the spatial anticorrelation between temperature changes and latent heating. It is shown that all three balance conditions reproduced the thermal structure of the easterly waves that passed over GATE during Phase III. Despite the differences in formulation and form, the simpler standard balance equations were as accurate as the first-order divergence equation in diagnosing the temperature field. The central result of the analysis is that the lower cold-core temperature anomaly observed in the near-trough region of easterly wave disturbances is not a direct consequence of the distribution of latent heat released by cumulus clouds, but reflects instead a balance of forces that dominate the momentum field and that the agreement between the observed and diagnosed temperature fields is dominated by the rotational component of the flow. This has possible implications for a first-order model of the interaction between cumulus-scale and large-scale equatorial wave motions, and for the distinction between developing and nondeveloping easterly waves in terms of the ambient vorticity field, which may aid future numerical investigations of tropical cyclogenesis.

1. Introduction

Despite studies performed to understand the processes by which the latent heat released inside cumulus clouds may be imparted to the large-scale flow (e.g., Ooyama 1971; Fraedrich 1973; Yanai et al. 1973; Arakawa and Schubert 1974; Nitta 1977; Johnson 1976; Cho 1977; etc.), it is still not known exactly how cumulus heating leads to the observed temperature field of large-scale equatorial systems, such as easterly waves. The thermal structure of a tropical easterly wave has some unexpected features. As pointed out by Cho and Jenkins (1987), the temperature field of these waves is complex, both in the vertical and horizontal directions. Temperature fluctuations are practically negligible: ~0.6°C at most, a fraction of a degree. These temperature changes are small despite radiative heating rates of ~2°C day^{-1}. Furthermore, in the convectively active sectors of the wave, where latent heating by cumulus cloud activity is ~10°C day^{-1}, temperature changes are *negative*. These disturbances are typically cold cored at lower-tropospheric levels in regions where condensation heating released by convection is greatest. This is inconsistent with the view that the thermal structure of these waves is a direct reflection of the distribution of latent heat released by cumulus clouds and that the generation and maintenance of these disturbances can be explained in terms of thermodynamical forcing by cumulus convection alone.

According to Cho and Jenkins (1987) these features of tropical easterly waves suggest that the air circulations induced by the heating due to latent heat release maintain certain properties that permit the air to retain as thermal energy only a very small fraction of the heat supplied by cumulus clouds. Although latent heat released inside cumulus clouds warms cloud air by ~2 K, its effect on the large-scale temperature field is small. This is because the total area covered by clouds, or Σ fractional cloud coverage, is typically ~1% to 10%. Therefore, although the difference in temperature between the environmental air and cloud air is $\Delta T \sim 2$ K, the temperature change on the large scale is $\Sigma\Delta T \sim 0.02$ to 0.2 K.

Thermodynamic energy considerations given in Cho and Jenkins (1987) indicate that the large-scale temperature field is influenced by cumulus activities in the following way: The vertical transport of mass takes place mainly inside clouds, and cumulus cloud activities induce subsiding motion in the cloud environment, adiabatic compression, and subsequent large-scale

Corresponding author address: Dr. Mary Ann Jenkins, Dept. of Earth and Atmospheric Science, York University, 149 Petrie Science Building, 4700 Keele Street, North York, ON M3J 1P3, Canada.

warming. How large is this subsidence warming in the cloud environment? In the Tropics, the Coriolis parameter is small and the Rossby number is of the order unity or greater. Scale analysis of the large-scale momentum equation indicates that hydrostatic temperature changes can be only a fraction of a degree, in agreement with observations. Consequently, even though diabatic heating in the thermodynamic energy equation produces cloud mass flux and large-scale vertical motion, the vertical velocity field and the change of temperature in the cloud environment are extremely weak. The thermodynamic energy equation is, as a result, limited in usefulness as a prognostic equation for temperature change in synoptic-scale tropical circulations. Furthermore, since $\Sigma\Delta T \sim 0.2$ K, subsidence warming in the cloud environment is restricted to ~ 0.2 K day^{-1}, and the vertical motion in the cloud environment is essentially zero, regardless of the strength of convective activity. Vertical transport of mass takes place only within clouds, and the mean horizontal divergence in the cloud environment is an order of magnitude smaller than both the large-scale relative vorticity and the large-scale horizontal divergence. To a first-order approximation, the airflow in the environmental area between cumulus clouds is nondivergent in the tropical atmosphere, independent of the strength of cumulus convection.

What relationship is required to maintain these properties of the mean circulation in a synoptic-scale tropical disturbance? According to Cho and Jenkins (1987), it is a balance between the mean pressure field, the large-scale and cloud–environment mean dynamic properties, and the pressure forcing at cloud boundaries [i.e., their Eq. (25)]. It was noted, however, that unless the nature of the pressure forcing at cloud boundaries is understood and the physical processes it represents explicitly parameterized, this general balance condition cannot be put into practice. If, however, the tropical system is slowly evolving, where the growth rate of the wave is much less than its angular frequency, then the relationship that describes an *approximate* balance condition—in which the mean divergence tendency is relatively small by virtue of a near balance between the divergence of the large-scale pressure gradient force and the divergence of the large-scale inertial forcing—is

$$\nabla^2\phi = -\frac{\partial\delta}{\partial t} - 2\mathbf{V}\cdot\nabla\delta + \frac{\zeta^2}{2} + f\zeta - \frac{3\delta^2}{2} - \frac{A_s^2}{2} - \frac{B_s^2}{2} - \beta u, \quad (1a)$$

a first-order divergence equation in pressure p coordinates. The notation is standard where ϕ is geopotential height, ∇ the horizontal gradient operator, $\mathbf{V}$ the horizontal velocity field, and β the latitudinal variation of the Coriolis parameter f. Here $\zeta = \partial v/\partial x - \partial u/\partial y$ is the vertical component of relative vorticity, $\delta = \partial u/\partial x + \partial v/\partial y$ the horizontal divergence, and $A_s = \partial u/\partial y + \partial v/\partial x$ and $B_s = \partial u/\partial x - \partial v/\partial y$ are, respectively, the horizontal shearing and stretching deformations of the wind field. Here u and v are, respectively, the east–west and north–south components of $\mathbf{V}$. Hydrostatic considerations give

$$-\frac{R}{p}\nabla^2 T = \frac{\partial}{\partial p}\left[-\frac{\partial\delta}{\partial t} - 2\mathbf{V}\cdot\nabla\delta + \frac{\zeta^2}{2} + f\zeta - \frac{3\delta^2}{2} - \frac{A_s^2}{2} - \frac{B_s^2}{2} - \beta u\right], \quad (1b)$$

which allows a physical interpretation of the relationship between the mean momentum field and T, the mean temperature field, in the tropical atmosphere. Cho and Jenkins (1987) show how it is possible, without a specific formulation of the forcing at the boundaries of clouds, to derive (1), if it is assumed that the flow in the cloud environment is nondivergent and the horizontal eddy flux of momentum associated with cumulus clouds can be neglected.

In an attempt to verify (1b), the thermal structure of tropical easterly waves that are slowly evolving or in steady state was constructed by Cho and Jenkins (1987) from the dynamic fields of the composite easterly wave presented in Thompson et al. (1979). Even though the Cho and Jenkins (1987) result compared reasonably well to the observed temperature field, there were problems with their analysis. Because the data came directly from Thompson et al. (1979), a considerable number of approximations were necessary: since no information was provided about the deformation field, terms $-A_s^2/2$ and $-B_s^2/2$ in (1b) were neglected; the time change term was estimated by a simple wave advection where the phase speed was set a priori in agreement with the Thompson et al. (1979) results; although the composite wave clearly has a meridional structure as shown in Reed et al. (1977), only the east–west cross section of the composite wave was presented by Thompson et al. (1979), and the meridional gradients in the Cho and Jenkins (1987) analysis of (1b) were therefore neglected; for the same reason, the Laplacian of the wave perturbation field was approximated by set meridional and zonal wavenumbers in agreement with observations. It was therefore not possible with these approximations to present the composite structure of the individual terms in (1b) to examine what physical effect each possibly has on the temperature field in this type of disturbance. A more careful analysis, using original observational data to qualify every term in the balance equation, was suggested.

The purpose, therefore, of this study is to provide a more complete rendition of the simple balance equation than that of Cho and Jenkins (1987) and, in the process, identify what effects in the divergence equation are responsible for the observed temperature field and suggest what possible implications these effects have to a slowly evolving tropical disturbance.

The Cho and Jenkins equation is almost the full divergence equation for synoptic-scale flow where no parameterization of convective cloud effects is explicitly required. Although it was presented in a comprehensive and self-consistent theoretical framework for easterly wave circulations, it is similar in form to the simpler standard nonlinear and linear balance conditions for adiabatic frictionless flow at low latitudes. Therefore, comparisons between the temperature field diagnosed by the divergence equation and fields diagnosed by the standard balance equations are also made to understand the reason for the historical success of the latter equations in simulating the behavior of these systems. It will be shown that, in each case, the lower-level cold core in the trough region of a convectively active wave is dominated by vorticity, the rotational component of the flow.

2. Data source and analysis

To reexamine the Cho and Jenkins (1987) divergence equation (1) for slowly evolving synoptic-scale disturbances in the Tropics, A/B- and B-scale upper-air data collected during Phase III (30 August to 18 September 1974) of the Global Atmospheric Research Program (GARP) Atlantic Tropical Experiment (GATE) are used. Phase III upper-air temperature, relative humidity, wind speed and direction, and height data were provided on tape by the U.S. World Data Center in Ashville, North Carolina. The details of the data processing method are reported in Jenkins et al. (1982). In this analysis a three-hourly time interval is used and at every three-hourly sounding, all available ship observations, interpolated to constant pressure levels, were fit using a least-squares method to a second-order polynomial. For any observation γ it is assumed that

$$\gamma = Ax^2 + By^2 + Cxy + Dx + Ey + F, \quad (2)$$

where x and y are the east–west and north–south coordinates, respectively. The upper-case roman letters of the polynomials of observations are the best-fit coefficients in the least-squares sense and were used to determine analytically the needed parameters.

During Phase III, a regular succession of six well-developed tropical easterly waves, which originated over western Africa, passed over the GATE area. They were cyclic in nature, each having approximately constant and similar phase speeds and angular frequencies, and maximum growth rates not exceeding Cho and Jenkins's (1987) definition of "slowly evolving" disturbances. These waves are therefore suitable for compositing and examination by (1). The composite technique adopted by Thompson et al. (1979) is again employed to produce the structure of a typical tropical easterly wave.

Compositing was done as follows. Every sounding was assigned one of eight wave categories in accordance with the wave phase classification given in Thompson et al. (1979). Wave category means produced a wave composite representing eight wave regions over one wavelength of a tropical easterly wave. Categories 2, 4, 6, and 8 designate regions of maximum northerly winds (N), wave troughs (T), maximum southerlies (S), and wave ridges (R) at the 700-mb level, respectively. Categories 1, 3, 5, and 7 are intermediate regions. Cumulus cloud activity was usually observed to be greatest slightly ahead of and in the trough region, and heavy precipitation generally occurred in regions 2 to 5. Finally, wave components were found by subtracting the overall GATE Phase III mean from the composite wave category mean, a step taken (following Stevens 1980) to reduce any possible systematic errors in the dataset. To illustrate plainly the wave structure of each meteorological field, Phase III wave composite fields are displayed as vertical east–west cross sections over one wavelength of the wave. In each vertical cross section are dashed lines indicating the trough (ridge) axis as the region of the wave where the amplitude of vorticity is a maximum (minimum).

Before discussing the results, it should be noted that there are both advantages and disadvantages with the compositing technique generally. Although there may be difficulties calculating terms in the divergence equation using individual, three-hourly rawinsonde measurements, wave compositing (averaging) has the advantage of reducing the expected error in the calculation by a factor of $1/\sqrt{N}$, where N is the number of samples going into the composite. For GATE Phase III, this factor ranges from 0.20 (wave category 6, $N = 26$) to 0.25 (wave categories 1 and 3, $N = 16$). Compositing works reasonably well for essentially linear quantities, but quadratic variables can be seriously and systematically underestimated by this method, especially if the individual quantities are first averaged and then squared. In this analysis individual quantities were first squared and then composited in an attempt to prevent severely underestimating quadratic terms. The wave composites are, following Thompson et al. (1979), based on the wave structure at the 700-mb level, which contributes to discrepancies at upper levels. Furthermore, determining the geopotential field involved integration of the hydrostatic equation; the accuracy of surface values and the accumulation with height of observational error in the temperature and humidity data produce increasingly greater and unrealistic values of ϕ at upper levels.

Error in the data increasing with height, together with the possible underestimation of squared quantities in the composite approach and the 700-mb wave category assignment, can explain the poor consistency found at upper levels, above 350–400 mb, in the present analysis. It is emphasized, therefore, that the study concentrates on the middle and lower troposphere where the data and the compositing technique provide the strongest support for the results presented; the con-

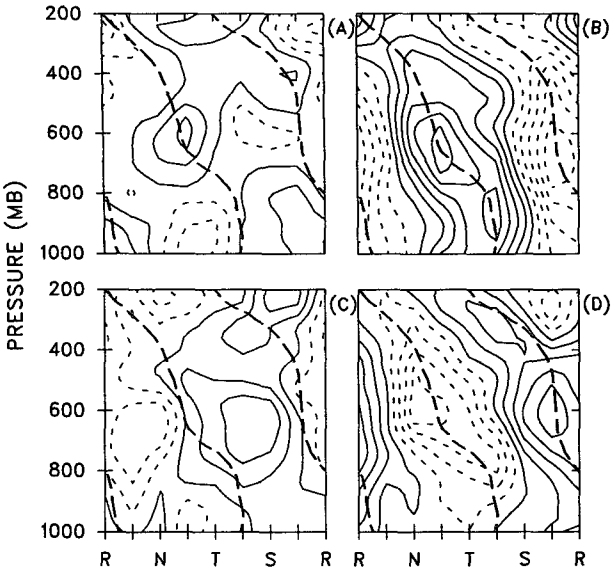

FIG. 1. Vertical cross sections of the (a) horizontal divergence δ, (b) vertical component of the relative vorticity ζ, and horizontal deformation (c) shearing A_s and (d) stretching B_s, over one wavelength of the wave. The values shown are deviations from the Phase III mean. Solid (dashed) contours are positive (negative) amplitudes. Heavy dashed lines indicate wave trough and ridge axes. Contour interval: 2.5×10^{-6} s^{-1}.

clusions are based on qualitative or relative, not quantitative, agreement or consistency in behavior.

a. *Mean fields*

Wave composites of the mean divergence δ, relative vorticity ζ, and deformation shearing A_s and stretching B_s are shown in Fig. 1. Generally, the ζ and δ wave composites are similar in magnitude and behavior to the composites of Thompson et al. (1979, Figs. 12, 13) and Reed et al. (1977, Fig. 8). The ridge and trough axes are nearly vertical below 800 mb, sloping westward above, and the wave vorticity maximum at the 650-mb level is one category ahead of the surface trough (Fig. 1b). The behavior of the wave composite of B_s is opposite that of ζ; regions of negative (positive) B_s (Fig. 1d) correspond to positive (negative) areas of ζ (Fig. 1b) throughout, while at every level wave amplitudes of maximum (minimum) B_s closely follow the ridge (trough) axis of ζ. The wave component of A_s is negative (positive) ahead of (behind) the trough axis below 300 mb and counterwise above (Fig. 1c).

The most irregularly patterned wave field in Fig. 1 is the mean divergence δ. Wave divergence varies considerably in the vertical, particularly over the trough region (Fig. 1a). Convergence is most significant in the lower troposphere below 750 mb, just above and before the surface trough. Relatively strong divergence takes place in the middle troposphere, between 750 and 500 mb. Divergence occurs again in the upper troposphere, around 200 mb, just above a shallow layer of weak convergence. Between 800 and 500 mb, divergence increases as the trough axis approaches and decreases as the ridge axis approaches.

Figure 1 shows that the rotational and deformation stretching components of the flow are large compared to divergence or deformation shearing. The wave components of ζ, B_s, and δ and A_s peak at ~650 mb, the level of the African easterly jet, reaching, respectively, maximum amplitudes of ~15 to 20 $\times 10^{-6}$ s^{-1}, ~10 $\times 10^{-6}$ s^{-1}, and ~5 $\times 10^{-6}$ s^{-1}. Figure 1 shows that above cloud base (~900 mb) and below 300 mb, the wave amplitude of divergence is smaller in magnitude than that of vorticity by a factor of ~3, indicating that, although the mean divergence is not negligible, these waves are quasi nondivergent throughout a substantial depth of the troposphere.

Figure 3 of Thompson et al. (1979) shows the mean zonal flow in the GATE area: strong, low-level monsoon westerlies just above the surface, the easterly African jet between ~600 and 700 mb, and an upper-tropospheric easterly jet at ~200 mb. The steering level is located at ~250 mb where the mean zonal wind approaches the average wave phase speed of -8 m s^{-1}. Air motion relative to the waves is therefore from the west below ~250 mb, and from the east between ~250 and 125 mb.

b. *The first consistency check of the approximate balance condition: Eq. (1a)*

Figure 2 shows wave composites of $\nabla^2\phi$ and the net effect of the sum of the terms on the right side of (1a).

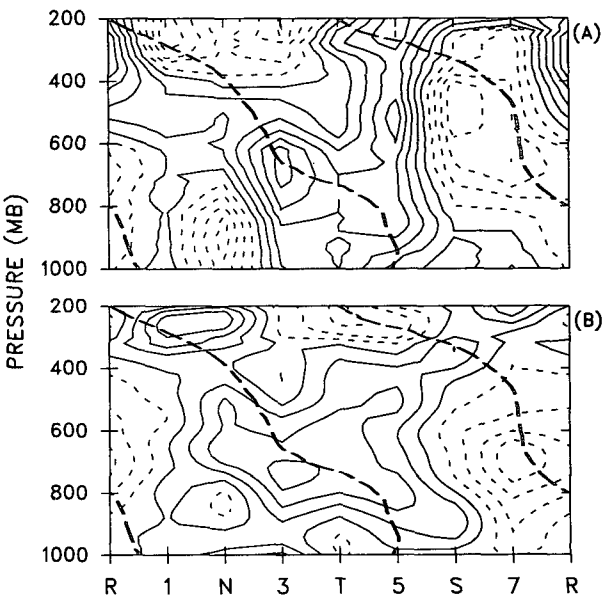

FIG. 2. Same as Fig. 1 except for (a) $\nabla^2\phi$ and (b) the net result of the right side of (1a). Contour interval: 1×10^{-10} s^{-2}.

In Fig. 2a, positive and negative $\nabla^2\phi$ at the trough and ridge axes indicate, respectively, extensive regions of low and high pressures below 350–400 mb, and in Fig. 2b the net effect of the sum of the terms on the right side of (1a) produces the desired positive and negative effects in areas of lower and higher pressure throughout the layer. Here $\nabla^2\phi$ reaches amplitudes of ~4 to 5 $\times 10^{-10}$ s^{-2}, somewhat larger than the amplitudes of ~3 to 4 $\times 10^{-10}$ s^{-2} seen in Fig. 2b.

Above 350–400 mb, however, there is little similarity between Figs. 2a and 2b. As discussed previously, these large discrepancies at upper levels are due to unreliability in the data and the compositing method. The large amplitudes above 350–400 mb in Fig. 2b indicate that there were problems computing reasonable $2\mathbf{V}\cdot\nabla\delta$ values with the available wind observations.

As shown in Fig. 1, in most regions of the composite easterly wave the magnitude of ζ is approximately three to four times the magnitudes of δ and A_s, and, consequently, not all terms in (1a) are equally significant.

Wave composites of the terms on the right side of (1a) are given in Fig. 3. Here $-3\delta^2/2$ (Fig. 3d) is significant only below 850 mb in the region of strong convergence ahead of the surface trough. Otherwise $-3\delta^2/2$ is practically negligible and, along with the wave components of $-A_s^2/2$ (Fig. 3e), $-B_s^2/2$ (Fig. 3f), and $-\beta u$ (Fig. 3h), reaches values of only ~5 $\times 10^{-11}$ s^{-2} and only over a limited area. The wave components of $-\partial\delta/\partial t$ and $-2\mathbf{V}\cdot\nabla\delta$ (Figs. 3a and 3b) vary considerably in both the vertical and horizontal directions and are relatively substantial, with peak amplitudes of ~15 $\times 10^{-11}$ s^{-2} below 350 mb. The tendency $-\partial\delta/\partial t$ is similar in behavior to δ except that it is shifted eastward by approximately one-quarter of a wavelength: Figs. 1a and 3a show, respectively, areas of positive (negative) $-\partial\delta/\partial t$ about one-fourth of a wavelength east of areas of divergence (convergence). To some extent $-2\mathbf{V}\cdot\nabla\delta$ (Fig. 3b) is negatively correlated with $-\partial\delta/\partial t$ (Fig. 3a), and although individually significant, the sum of $-2\mathbf{V}\cdot\nabla\delta$ and $-\partial\delta/\partial t$ (not shown) is comparatively *small,* typically less than ~15 $\times 10^{-11}$ s^{-2} below 350 mb.

Wave amplitudes of $\zeta^2/2$ (Fig. 3c) and $f\zeta$ (Fig. 3b) are quite significant and similar in structure below 350–400 mb, reaching, respectively, wave maxima of ~15 and 25 $\times 10^{-11}$ s^{-2}, and consequently the sum of the wave components of $\zeta^2/2$ and $f\zeta$ (not shown) is comparatively *large* below 350 mb. Combined, $\zeta^2/2 + f\zeta$ have amplitudes greater than 15 $\times 10^{-11}$ s^{-2} over broad areas along the trough and ridge axes. Above 350–400 mb, the behavior and magnitude of the wave components of $\zeta^2/2$ change, becoming almost negligible and positive (negative) along the ridge (trough) axis, an unusual pattern not seen in the wave composite of $f\zeta$.

To summarize, a comparison between Figs. 2 and 3 indicates that it is largely $\zeta^2/2$ (Fig. 3c) and $f\zeta$ (Fig. 3g) in (1a) that are responsible for the observed wave behavior of $\nabla^2\phi$ (Fig. 2a) below 350–400 mb. No other terms, or combination of terms, on the right-hand side of (1a) show the same steady continuity with the behavior and magnitude of $\nabla^2\phi$.

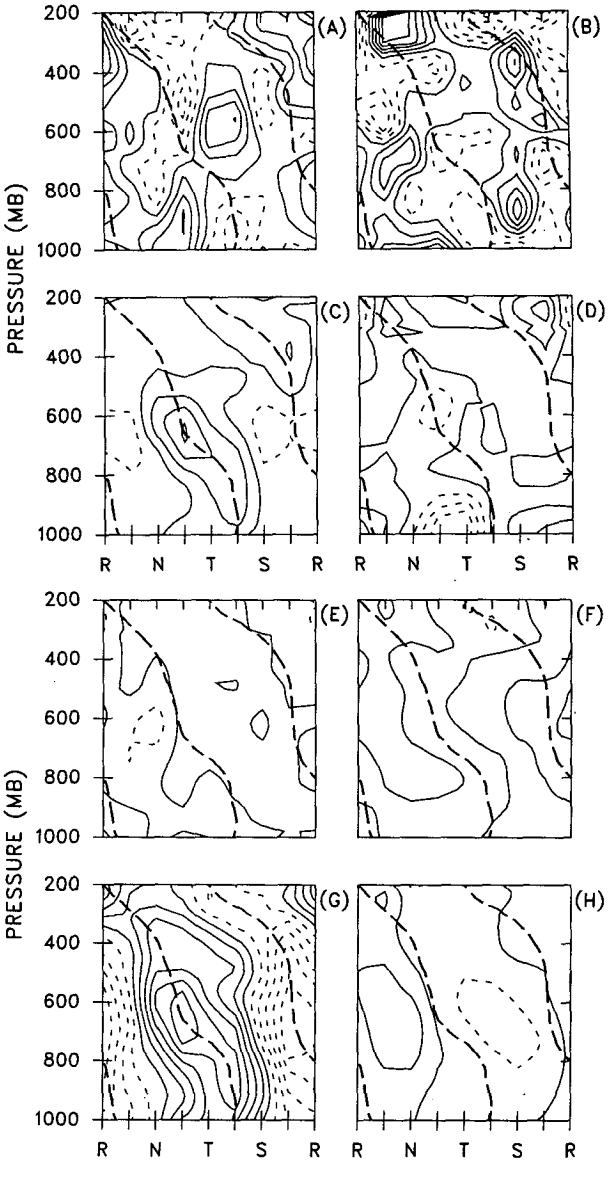

FIG. 3. Same as Fig. 1 except for (a) $-\partial\delta/\partial t$, (b) $-2\mathbf{V}\cdot\nabla\delta$, (c) $\zeta^2/2$, (d) $-3\delta^2/2$, (e) $-A_s^2/2$, (f) $-B_s^2/2$, (g) $f\zeta$, and (h) $-\beta u$. Contour interval: 5 $\times 10^{-11}$ s^{-2}.

c. *The second consistency check of the approximate balance condition: Eq. (1b)*

The wave composites of $\nabla^2\partial\phi/\partial p$, $-R/p\nabla^2T$, and the right side of (1b) given in Fig. 4 show fields of complex structure that vary greatly in both vertical and horizontal directions. Below 350–400 mb the agreement between the three wave composites is generally good. Even though there are some differences in mag-

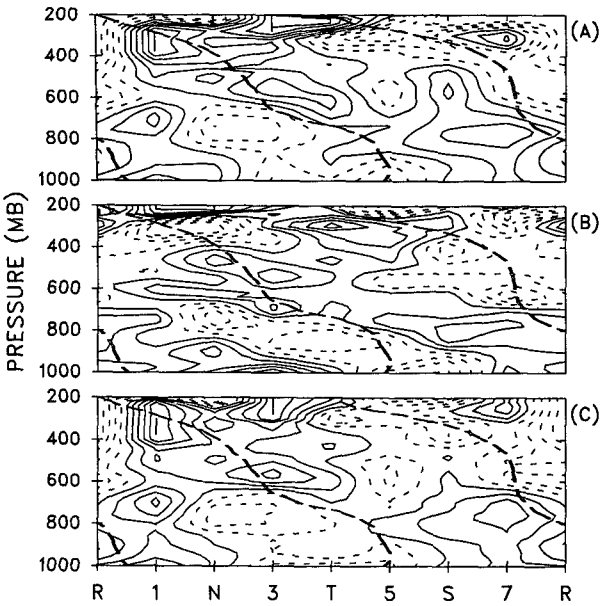

FIG. 4. Same as Fig. 1 except for (a) $\partial\nabla^2\phi/\partial p$, (b) the net results of the right side of (1b), and (c) $-R/p\nabla^2 T$. Contour interval: 1 $\times 10^{-12}$ mb^{-1} s^{-2}.

nitude and shape of contours, these results indicate that (1b) successfully produces correct outlines of positive and negative wave amplitudes of $\nabla^2\partial\phi/\partial p$ and $-R/p\nabla^2 T$ throughout this layer. Above 350 mb agreement diminishes. As in Fig. 2, the large negative and positive amplitudes seen in Fig. 4b above 350 mb do not accompany negative and positive amplitudes of $\nabla^2\partial\phi/\partial p$ and $-R/p\nabla^2 T$. However, the overall agreement between the profiles below 350–400 mb does indicate that the balance condition is applicable to the dynamics of a typical tropical disturbance throughout a substantial depth of the troposphere. The differences between amplitudes of $\nabla^2\partial\phi/\partial p$ and $-R/p\nabla^2 T$ are due primarily to the error involved in determining the geopotential from observational data.

To examine whether (1b) represents the relationship between the thermal field and the momentum field of an easterly wave, we follow Cho and Jenkins's (1987) procedure and assume that the Laplacian of the wave perturbation is simply $\nabla^2 \approx -(k_x^2 + k_y^2)$, where the meridional wavenumber $k_y \approx 1.7 \times 10^{-6}$ m^{-1}, and the zonal wavenumber $k_x \approx 2.5 \times 10^{-6}$ m^{-1}. Taking the composite wave components in Fig. 4b and multiplying by $p/R(k_x^2 + k_y^2)$ produces a temperature field based on the balance condition and the first-order divergence equation. It is possible that the agreement with observations would be even better were the true Poisson equation solved for temperature. Errors are introduced by this approximation to the Laplacian. In particular, because the fields are not precisely wavelike, the approximation provides a smoothing effect.

The result is shown in Fig. 5b and can be compared to the observed temperature field shown in Fig. 5a. It is apparent that the first-order divergence equation provides a qualitatively correct outline of the major regions of warm and cold masses of air. With very few exceptions the placement of the warm and cold cores agrees quite well with observations. Temperature perturbations are weak, and the lower-level cold core and mid- to upper-level warm core are typical of the vertical thermal structure in the trough region of a tropical easterly wave. In this region, temperature perturbations are negative below 650 mb and positive above 650 mb. Further, although core amplitudes computed using (1b) are generally stronger than observed (e.g., −0.8 K instead of −0.6 K in the cold-core trough region at 800 mb), they are still a fraction of a degree. These differences, as pointed out by Cho and Jenkins (1987), are no more significant than differences between two temperature fields obtained by two separate analyses of the same set of observational data.

To decide which terms on the right side of (1b) are responsible for the unusual thermal structure of a tropical easterly wave (i.e., the lower-level cold core in the trough region of the wave where cumulus activity and latent heat release are considerable), wave composites of each term on the right side of (1b) were also computed (not shown). It is found that the wave components of the vertical variations of $-A_s^2/2$, $-B_s^2/2$, and $-\beta u$ are small, considerably less than $\sim 0.5 \times 10^{-12}$ sec^{-2} mb^{-1} throughout, and the vertical variation of $-3\delta^2/2$ is significant, and positive, only below 850 mb just ahead of and at the surface trough, while the ver-

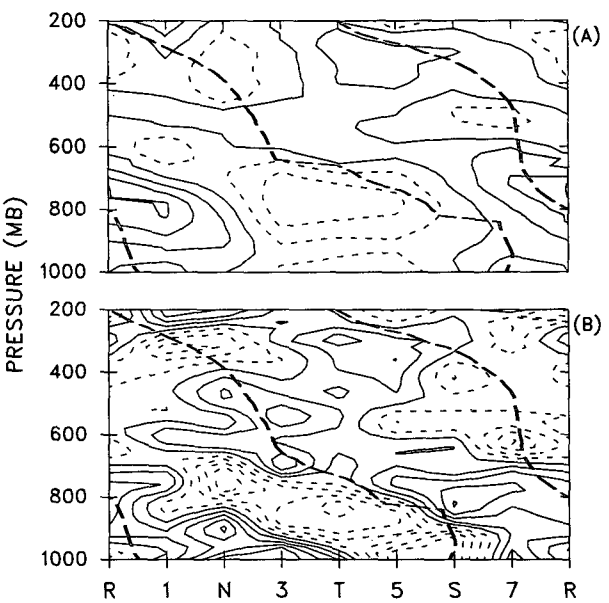

FIG. 5. Same as Fig. 1 except for (a) observed temperature and (b) temperature diagnosed by the divergence equation (1b). Contour interval: 0.2 K.

tical variations of $\zeta^2/2, f\zeta, -\partial\delta/\partial t$, and $-2\mathbf{V}\cdot\nabla\delta$ are substantial.

Figure 6a shows that, combined, the effects of $\partial(\zeta^2/2)/\partial p$ and $\partial(f\zeta)/\partial p$ in (1b) are large, with amplitudes greater than $\sim 1 \times 10^{-12}$ sec^{-2} mb^{-1} over extensive regions of the wave. Figure 6b shows that, combined, the effects of $-\partial(\partial\delta/\partial t)\partial p$ and $-\partial(2\mathbf{V}\cdot\nabla\delta)\partial p$ in (1b) are also equally large, especially above 350–400 mb, and very variable in behavior. What is important here, however, is that below 650 mb, just west of and at the trough axis, wave amplitudes of $-\partial(\partial\delta/\partial t + 2\mathbf{V}\cdot\nabla\delta)\partial p$ are extensively *positive,* while wave amplitudes of $\partial(\zeta^2/2 + f\zeta)/\partial p$ are extensively *negative* in this region of the wave. A comparison between Figs. 6a and 5a indicates that the negative and positive wave amplitudes of $\partial(\zeta^2/2 + f\zeta)/\partial p$ agree quite well with the placement of the cold and warm temperature anomalies below and above 650 mb in the trough region of the wave. No other terms, or combination of terms, on the right-hand side of (1b) show the same steady continuity with the behavior of the observed temperature field of the wave. Below 400 mb, Figs. 4c and 6a show a definite correlation between the wave structure of $-R/p\nabla^2 T$ and the momentum forcing by $\partial(\zeta^2/2 + f\zeta)/\partial p$.

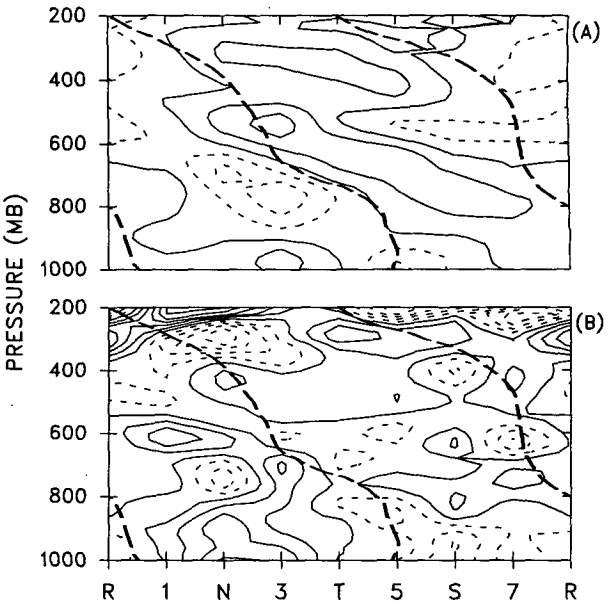

FIG. 6. Same as Fig. 1 except for (a) $\partial(\zeta^2/2 + f\zeta)/\partial p$ and (b) $-\partial(\partial\delta/\partial t + 2\mathbf{V}\cdot\nabla\delta)/\partial p$. Contour interval: 1×10^{-12} mb^{-1} s^{-2}.

3. A comparison with the standard linear and nonlinear balance equations

Numerical investigations of tropical easterly wave motions using simple balanced models that assume that the irrotational component of the wind is zero and that the heating and frictional effects are negligible have produced satisfactory results (e.g., Krishnamurti and Baumhefner 1966). These numerical simulations, however, offer no theoretical explanation as to why adiabatic and frictionless balanced models apparently contain dynamics adequate to describe convectively active motion fields in low latitudes. There are differences between (1) and the standard nonlinear and linear balance equations, but it is possible, using the composite technique, to compare these equations to (1) here to see why, despite the differences, standard theory does a good job simulating easterly wave behavior.

Assuming that the effects of subscale eddies associated with cumulus cloud activities and adiabatic heating are negligible and that the magnitude of the nondivergent component of the wind velocity $\mathbf{V}_\psi$ is much greater than the irrotational, the pressure-coordinate form of the standard divergence equation for equatorial synoptic-scale motions can be written

$$-2\mathbf{J}(u_\psi, v_\psi) - f\zeta + \beta u_\psi + \nabla^2\phi = 0, \qquad (3)$$

where the nondivergent component is expressed in terms of the streamfunction ψ defined by $\mathbf{V}_\psi = \mathbf{k} \times \nabla\psi$ and $\mathbf{J}$ is the Jacobian (Haltiner 1979). This is the standard nonlinear balance equation, which implies a continual balance between the rotational wind component and the geopotential field. If $2\mathbf{J}(u_\psi, v_\psi)$, the nonlinear term, is omitted, then (3) becomes

$$-f\zeta + \beta u_\psi + \nabla^2\phi = 0, \qquad (4)$$

the standard linear balance equation. Comparing (3) to (1), which can be rewritten as

$$\frac{\partial\delta}{\partial t} + 2\mathbf{V}\cdot\nabla\delta + 2\delta^2 - 2\mathbf{J}(u, v) - f\zeta + \beta u + \nabla^2\phi = 0, \qquad (5)$$

where the Jacobian term is

$$2\mathbf{J}(u, v) = \frac{1}{2}(\zeta^2 + \delta^2 - A_s^2 - B_s^2),$$

shows that the differences between (3) and (5) are the total wind velocity $\mathbf{V}$ as opposed to $\mathbf{V}_\psi$ and the addition of terms $\partial\delta/\partial t$, $2\mathbf{V}\cdot\nabla\delta$, and $2\delta^2$ in (5).

To determine $\mathbf{V}_\psi$ in (3) and (4), the equation $\nabla^2\psi = \zeta$ was solved by finite-difference approximations: using (2), u and v wind components were established every 25 km throughout a 1000 km × 1000 km domain, centered over the GATE area; the boundary conditions were necessarily $u = -\partial\psi/\partial y$ and $v = \partial\psi/\partial x$, where u, v are components of the total wind field. GATE area averages were taken and the composite analysis done in the same manner as in section 2. The resulting temperature fields diagnosed using (3) and (4) are shown in Fig. 7. Here wavenumbers k_x and k_y from section 2 were used to approximate the wave Laplacian.

Comparing Fig. 7 to the observed temperature field in Fig. 5a shows that both the nonlinear and linear balance equations provide qualitatively correct outlines of

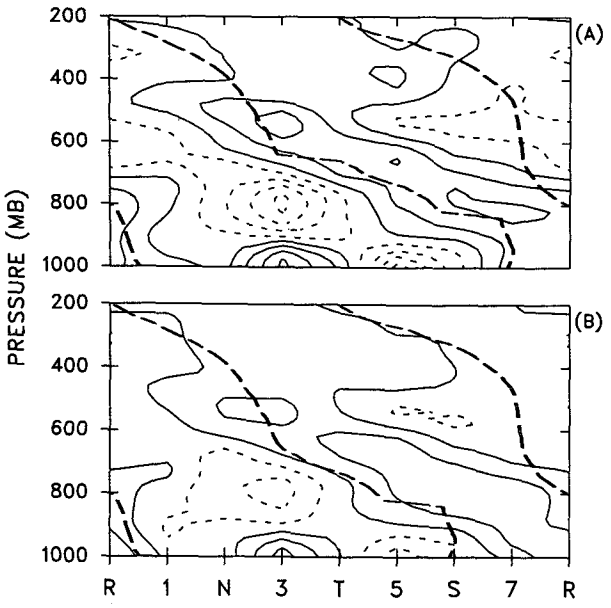

FIG. 7. Same as Fig. 1 except for temperature diagnosed by (a) the nonlinear balance (3), and (b) the linear balance (4). Contour interval: 0.2 K.

the major regions of warm and cold masses of air below 350 mb. As in Fig. 5b, diagnosed temperature perturbations are weak, and the typical vertical thermal structure in the trough region of an easterly wave is reproduced; temperature perturbations are negative below 650 mb, ranging in amplitude from ~0.4 to 0.6 K, positive above 650 mb, with smaller amplitudes of ~0.2 K. Core amplitudes computed using (3) are generally stronger than observed (e.g., −0.8 K instead of −0.6 K in the cold-core trough region at 800 mb), and the agreement between observed and diagnosed temperature fields diminishes above 350 mb.

The overall agreement between the diagnosed and observed temperature profiles below 350–400 mb indicates that the standard nonlinear and linear balance equations retain the terms that are responsible for the unusual thermal structure of a convectively active easterly wave. The most significant contribution to the positive correlation between the observed and diagnosed temperature fields is due to the effects of the rotational component of the wind, which is contained in (4) by the $f\zeta$ term, and in (3) by this term and $\zeta^2/2$ of the Jacobian term. These terms are the only ones in the standard balance equations that provide the desired *negative* result to the temperature field at low levels in the trough region of the wave, in agreement with observations. As described in section 2, the wave components of the vertical variations of $A_s^2/2$, $B_s^2/2$, and βu are comparatively small throughout, and the vertical variations of $\delta^2/2$ is significant only just ahead of and at the surface trough. The observations (Fig. 1) also indicate that, although the wave divergence is not negligible, the contribution by the rotational component of the wind $\mathbf{V}_\psi$ to the balance condition is the more significant.

4. Discussion

The analysis of Eqs. (1), (3), and (4) suggests that it is the large-scale vorticity, the rotational component of the wind, that most strongly influences the behavior of the temperature field. The results presented in section 2c indicate that the wave structure of $-R/p\nabla^2 T$ corresponds solely to the behavior of $\partial(\zeta^2/2 + f\zeta)/\partial p$, and it is therefore the vertical variation of the large-scale vorticity field that is largely responsible for the thermal structure of tropical easterly waves. Under these conditions the connection between the temperature field and momentum forcing of a tropical easterly wave is most simply expressed by

$$-\frac{R}{p}\nabla^2 T \propto \frac{\partial \xi}{\partial p}. \tag{6}$$

This simple relationship is evident in the near-trough regions in Figs. 1b and 4c. Below 650 mb, ζ is increasing with height, and, in response, the concave upward curvature of the geopotential pressure surface increases with height throughout the wave layer $-R/p\nabla^2 T < 0$, and temperature perturbations are negative. Above 650 mb, ζ is decreasing with height, and, in response, the concave upward curvature of the geopotential pressure surface weakens with height throughout the wave layer $-R/p\nabla^2 T > 0$, and temperature perturbations are positive.

5. Concluding remarks

Direct observational evidence suggests that the first-order divergence equation and the standard nonlinear and linear balance equations can account for the observed temperature field in the tropical easterly waves that passed over GATE during Phase III.

The results suggest that the thermal structure of an easterly wave reflects not so much the distribution of latent heat released by cumulus clouds, but what is required to maintain the dynamic structure of the wave, which is always constrained by the "balance condition." A rather mechanical picture is suggested here, where the forcing immediately responsible for significant temperature changes in these disturbances is the vertical variation of the large-scale vorticity field. In the GATE area, the cold-core temperature anomaly observed near the surface below 650 mb before and during the passage of the surface trough is associated with the increase with height of the large-scale vorticity. The warm core above is associated with a decrease of vorticity with height throughout the layer.

The ultimate goal is to provide a model of the interaction between cumulus-scale and large-scale motion in which the large-scale flow provides convergence,

producing clouds and moisture, and the cumulus clouds act cooperatively to provide a driving large-scale energy source. Therefore, how to explain the previous paragraph in terms of convective activity and latent heat release? The connection can be seen in the study of GATE Phase III easterly waves by Jenkins and Cho (1991). According to Jenkins and Cho, evolution of the vorticity field in a synoptic-scale tropical disturbance is influenced primarily by vorticity advection and the development of large-scale divergence due to cumulus convective activity. As discussed previously, at low latitudes, where the Rossby number is of the order unity or greater, hydrostatic temperature changes in the cloud environment are restricted. As a result the effect of latent heating in the thermodynamic energy equation is, to a first-order approximation, to produce large-scale vertical motion. The vertical transport of mass, however, takes places only within clouds. At levels where a net horizontal convergence (or divergence) of the cloud mass flux exists, reflected on the synoptic-scale as the convergence (or divergence) of the mean wind, a positive (or negative) contribution is made to the total horizontal derivative of vorticity, resulting in a possible increase (or decrease) in the effective angular velocity of the air parcel due to vortex tube stretching (or shrinking) by cumulus clouds.

This suggestion for a first-order model of the interaction between cumulus-scale and large-scale motions is important because, if correct, it has direct bearing on what exactly future numerical modeling studies should be examining when investigating tropical cyclogenesis, that is, the change in the large-scale vorticity field due to cumulus convective activities and its effect on the lower-level cold-core temperature anomalies and structure of the geopotential/pressure field. Convection is most active in the trough region; here vorticity advection is weak, and low-level convergence due to convective activities can act most effectively to increase vorticity near the surface. Following the discussion in section 4, when the rotational component of the wind is strongest at the surface and decreases steadily with height, $\nabla^2\phi$, in response, increases positively; pressures near the surface drop; and the lower-level cold-core anomaly disappears. Under favorable conditions, the wave makes a transformation into a warm-core tropical depression.

The theory for synoptic-scale weather disturbances in the midlatitudes is greatly simplified by the existence of geostrophic balance. In these weather systems the velocity field is basically a rotational field with its vorticity one order larger in magnitude than divergence. Consequently, there is an approximate balance between the centrifugal acceleration of the rotational flow and the Coriolis and pressure gradient forces. It is not known whether a similar condition exists for atmospheric flow in tropical disturbances other than tropical cyclones. The analysis here of the three balance equations (1), (3), and (4) implies that for atmospheric flow in synoptic-scale convectively active tropical wave disturbances a similar condition exists that dictates the thermal structure of these systems; the success of all three equations is contained in the terms $\nabla^2\phi, f\zeta$, and $\zeta^2/2$, which suggests a balance between the geopotential field and the rotational wind component.

The above remarks suggest that the thermal field arises in response to the vorticity field. Since there is a balance, cause and effect are not so clear, and this analysis is not able to provide evidence that the temperature is, in fact, adjusting to the wind. This is left for future study. This analysis is at least helpful in understanding qualitatively what processes are responsible for the seemingly paradoxical thermal structure of these systems. It has also shown why the simple frictionless adiabatic balance models in previous numerical investigations produce realistic-looking results. Indeed, the results in section 3 indicate that the divergence equation works no better than standard theory. Questions arising about the differences between the first-order divergence equation and the standard balance equations could possibly be answered by further, more refined, studies but will remain unanswered here. The divergence equation includes the local time change, which suggests the possibility of future prognostic use to examine the evolution of large-scale tropical circulation systems. The standard balance equations are, however, much simpler to apply and have the added advantage of reducing to the gradient wind balance, while the divergence equation does not except under the stringent condition of solid rotation. For now it must suffice to merely acknowledge the existence of an approximate balance and its importance to the thermal structure of tropical easterly wave disturbances.

Acknowledgments. This work has benefited greatly from the comments and suggestions of three anonymous reviewers and of Dr. Margaret LeMone. I would like to thank Professor Han-Ru Cho for his interest in this study, Dr. John McBride for his critical comments on an earlier draft, and Dr. Lloyd Shapiro for patiently answering my questions. This work was supported by research grants from the Natural Sciences and Engineering Research Council of Canada and the Canadian Atmospheric Environment Service.

REFERENCES

Arakawa, A., and W. H. Schubert, 1974: Interaction of a cumulus cloud ensemble with the large-scale environment: Part I. *J. Atmos. Sci.*, **31**, 674–701.

Cho, H.-R., 1977: Contribution of cumulus cloud life-cycle effects to the large-scale heat and moisture budget equations. *J. Atmos. Sci.*, **34**, 87–97.

——, and M. A. Jenkins, 1987: The thermal structure of tropical easterly waves. *J. Atmos. Sci.*, **44**, 2531–2539.

Fraedrich, K., 1973: On the parameterization of cumulus convection by lateral mixing and compensating subsidence: Part I. *J. Atmos. Sci.*, **30**, 408–413.

Haltiner, G. J., 1979: *Numerical Weather Prediction.* Wiley & Sons, 317 pp.

Jenkins, M. A., and H.-R. Cho, 1991: An observational study of the first-order vorticity dynamics in a tropical easterly wave. *J. Atmos. Sci.,* **48,** 965–975.

——, R. M. Bloxam, and H.-R. Cho, 1982: Further test of a theory of convective effects on the large-scale vorticity field in the tropics. *Atmos.–Ocean,* **20,** 207–226.

Johnson, R. H., 1976: The role of convective-scale precipitation downdraft in cumulus and synoptic-scale interactions. *J. Atmos. Sci.,* **33,** 1890–1910.

Krishnamurti, T. N., and D. Baumhefner, 1966: Structure of a tropical disturbance based on solutions of a multilevel baroclinic model. *J. Appl. Meteor.,* **5,** 396–406.

Nitta, T., 1977: Response of cumulus updraft and downdraft to GATE A/B-scale motion systems. *J. Atmos. Sci.,* **34,** 1163–1186.

Ooyama, K., 1971: A theory of parameterization of cumulus convection. *J. Meteor. Soc. Japan,* **49,** 744–756.

Reed, R. I., D. C. Norquist, and E. E. Recker, 1977: The structure and properties of African wave disturbances as observed during Phase III of GATE. *Mon. Wea. Rev.,* **105,** 317–333.

Stevens, D. E., 1980: Vorticity, momentum, and divergence budgets of synoptic-scale wave disturbances in the tropical eastern Atlantic. *Mon. Wea. Rev.,* **107,** 535–550.

Thompson, R. M., Jr., S. W. Payne, E. E. Recker, and R. I. Reed, 1979: Structure and properties of synoptic-scale wave disturbances in the intertropical convergence zone of the eastern Atlantic. *J. Atmos. Sci.,* **36,** 53–72.

Yanai, M., S. Esbensen, and I. Chu, 1973: Determination of average bulk properties of tropical cloud clusters from large-scale heat and moisture budgets. *J. Atmos. Sci.,* **30,** 611–627.